ACS central science

http://pubs.acs.org/journal/acscii

Research Article

Rapid and Accurate Visualization of Breast Tumors with a Fluorescent Probe Targeting α-Mannosidase 2C1

Kyohhei Fujita, Mako Kamiya, Takafusa Yoshioka, Akira Ogasawara, Rumi Hino, Ryosuke Kojima, Hiroaki Ueo, and Yasuteru Urano*

Cite This: ACS Cent. Sci. 2020, 6, 2217−2227

Read Online

ACCESS | Metrics & More | Article Recommendations | Supporting Information

ABSTRACT: Accurate detection of breast tumors and discrimination of tumor from normal tissues during breast-conserving surgery are essential to reduce the risk of misdiagnosis or recurrence. However, existing probes show substantial background signals in normal breast tissues. In this study, we focus on glycosidase activities in breast tumors. We synthesized a series of 12 fluorescent probes and performed imaging-based evaluation on surgically resected human breast specimens. Among them, the α-mannosidase-reactive fluorescent probe HMRef-αMan detected breast cancer with 90% sensitivity and 100% specificity. We identified α-mannosidase 2C1 as the target enzyme and confirmed its overexpression in various breast tumors. We found that fibroadenoma, the most common benign breast lesion in young woman, tends to have higher α-mannosidase 2C1 activity than malignant cancer. Combined application of green-emitting HMRef-αMan and a red-emitting γ-glutamyltranspeptidase probe enabled efficient dual-color, dual-target optical discrimination of malignant and benign tumors.

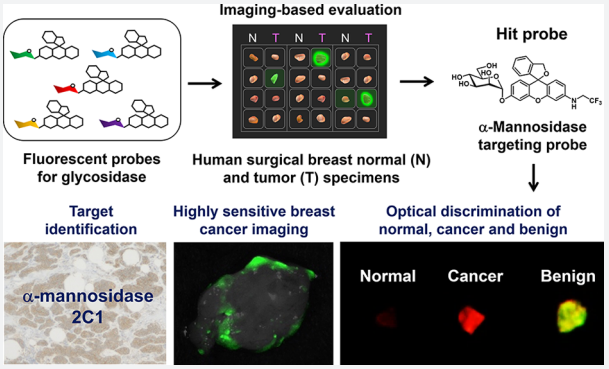

INTRODUCTION

Breast cancer is the most frequently diagnosed cancer in females worldwide, and about 2.1 million newly diagnosed cases were expected in 2018.[1] Breast-conserving surgery (BCS) has been established as the standard treatment for breast cancer,[2] but in BCS, it is extremely important to perform precise assessment of surgical margins intraoperatively in order to prevent local recurrence and to avoid the need for additional operations.[3] For this purpose, intraoperative pathological examination of hematoxylin and eosin (H.E)-stained frozen section is widely used due to its diagnostic accuracy. This traditional method of intraoperative frozen section analysis (IFSA), however, is challenged by considerations such as manpower, cost, and time (more than 40 min) to obtain a rapid diagnosis, especially regarding total-circumferential examination.[4,5] When the limited number of samples from surgical margins were examined for IFSA, the rate of false-negative inevitably increased. Therefore, there is an urgent need for a rapid and convenient method to evaluate the entire surface of the surgical margins.

Fluorescence-guided detection of cancer is one of the most promising approaches for intraoperative assessment of surgical margins, due to its high sensitivity, its real-time capability, and its ability to assess the entire surgical margins.[6−10] Several fluorescence probes for detecting the activity of proteases upregulated in breast cancer cells have been developed to visualize tumors rapidly and sensitively.[11−17] For example, we have focused on γ-glutamyltranspeptidase (GGT), whose activity is elevated in breast cancer, and developed a GGT-reactive fluorescent probe, gGlu-HMRG (Figure S1).[18,19] This probe successfully detected breast cancer in clinical specimens from patients after topical application.[9,20] However, in some cases, the probe shows substantial background fluorescence in normal breast tissues, which can potentially lead to false-positive results. Further, gGlu-HMRG is similarly activated in proliferative benign lesions and in malignant lesions and, therefore, cannot discriminate them.[9] Thus, we need to find an enzyme biomarker that can offer improved sensitivity and a methodology to achieve detection of malignant breast cancer.

In this report, we focused on glycosidases as candidate target enzymes. Glycosidases hydrolyze glycosidic linkages of glycoconjugates such as glycoproteins or glycolipids, whose expression in the intracellular milieu is known to be associated with tumor initiation, progression, and metastasis.[21−25] Therefore, increased expression levels of glycosidases can be a hallmark of cancer, and so these enzymes could be promising

Received: September 3, 2020
Published: October 29, 2020

https://dx.doi.org/10.1021/acscentsci.0c01189
ACS Cent. Sci. 2020, 6, 2217−2227

targets for cancer imaging. In order to detect upregulated glycosidase activities in breast cancer, we prepared a series of 12 fluorescent probes by incorporating different glycosides into our previously reported scaffold fluorophore, HMRef.[26−28] By applying these fluorescent probes to surgically resected breast tumor specimens from patients, we identified a new biomarker for breast tumors and confirmed that the tumors are specifically visualized by the probe.

RESULTS

Development of Fluorescent Probes for Various Glycosidase Activities. In order to design the desired fluorescent probes, we focused on our previously reported scaffold fluorophore for activatable fluorescence probes for glycosidases, HMRef. HMRef-based probes are nonfluorescent when conjugated to an enzyme substrate sugar moiety but are converted to highly fluorescent HMRef upon rapid one-step cleavage of their substrate moiety by the target enzyme, enabling sensitive detection of glycosidase activities in living cells.[28] Specifically, we prepared 12 fluorescent probes bearing different saccharide moieties: probe **1** (β-D-Glc), probe **2** (β-D-Gal), probe **3** (β-L-Gal), probe **4** (β-D-Xyl), probe **5** (α-D-Man), probe **6** (β-D-Fuc), probe **7** (α-L-Fuc), probe **8** (β-L-Fuc), probe **9** (α-D-Ara), probe **10** (α-L-Ara), probe **11** (β-D-GlcNAc), and probe **12** (β-D-GalNAc) (Figure 1; see Supporting Information (SI)). In order to evaluate whether these probes can visualize glycosidase activities in living cells, we applied them to perform live-cell fluorescence imaging of 22 cultured cancer cell lines (Figure 2a). The fluorescence intensity varied markedly among the cell line/probe pairs, which strongly suggests that each cell line has a distinct pattern of glycosidase activity (Figures 2b and S2). We confirmed that the observed fluorescence signals are due to reaction with the expected target enzymes by examining the effects of specific enzyme inhibitors on the fluorescence intensity of MCF7 cells after application of several probes (probe **1** for β-glucosidase, probe **2** for β-galactosidase, probe **5** for α-mannosidase, probe **7** for α-fucosidase, and probe **11** for β-hexosaminidase) (Figures 2c, d and S3−S5). Indeed, the fluorescence signals in cells were significantly suppressed in the presence of the corresponding inhibitors, indicating that they reflect enzyme activity in living cells. These results indicate that the synthesized probes can visualize glycosidase activities in living cells, and thus are promising candidates for fluorescence imaging-based screening of upregulated glycosidase activities in live breast cancer tissues in the clinical context.

Evaluation of Glycosidase Activities in Surgically Resected Breast Cancer Tissues. Next, we applied our fluorescent probes to surgically resected specimens of normal and breast cancer tissues. Specifically, frozen specimens of normal breast tissues and cancer tissues (invasive ductal carcinoma (IDC) or ductal carcinoma in situ (DCIS)) from the same patient were thawed and divided into pieces a few millimeters in size, and incubated with each of the 12 fluorescent probes to evaluate the corresponding glycosidase activities (Figure 3a). Some probes, such as probes **5** (α-D-Man) and **11** (β-D-GlcNAc), showed a significant and time-dependent fluorescence increase selectively in breast cancer tissues (Figure 3b, d, e and Figures S6, S7). Further, the fluorescence increase was significantly suppressed in the presence of an inhibitor of α-mannosidase or β-hexosaminidase, which strongly indicates that α-mannosidase and β-hexosaminidase activities are higher in cancer tissues than in normal tissue (Figure 3c). The sensitivity and specificity of these probes were calculated to be 90% and

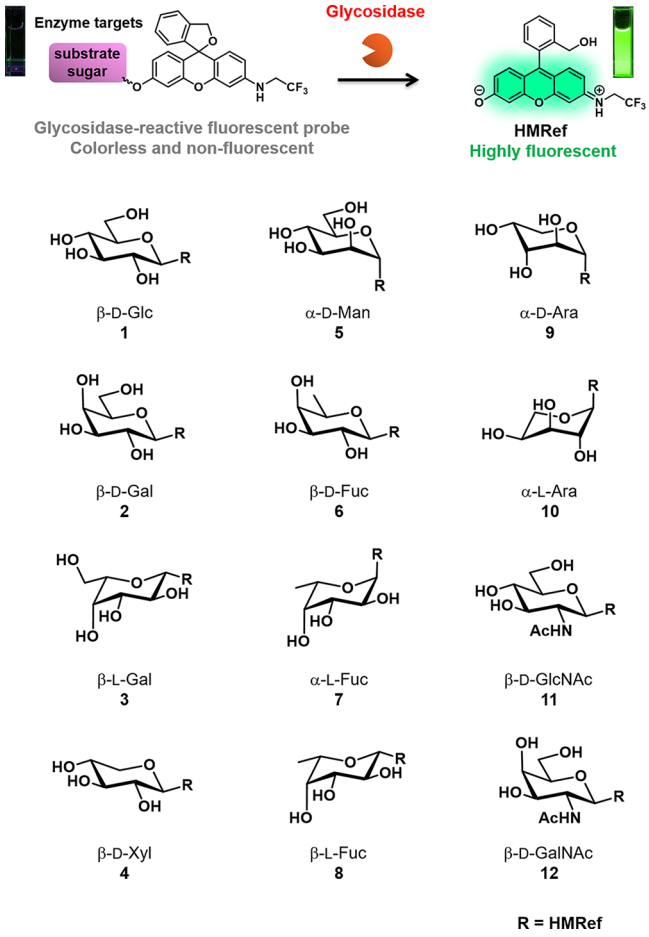

Figure 1. Fluorescent probes synthesized for the detection of glycosidase activities. These probes exist in colorless, nonfluorescent spirocyclic forms, but are converted to a colored, highly fluorescent hydrolysis product HMRef, which emits green fluorescence, upon reaction with the targeted glycosidase.

100% for probe **5** (α-D-Man) and 89% and 88% for probe **11** (β-D-GlcNAc), respectively, which are higher than those of gGlu-HMRG (80% and 79%, respectively) in this experiment (Table 1, S1 and Figure S8). Based on these results, we chose probe **5** (α-D-Man) as a promising imaging probe for breast cancer-specific imaging and named it HMRef-αMan. The absorbance and fluorescence changes of HMRef-αMan in the presence of α-mannosidase are shown in Figure S9.

Identification of α-Mannosidase 2C1 as a Novel Biomarker for Breast Cancer. Next, we examined which subtype of human α-mannosidase is responsible for the fluorescence increase in breast cancer by carrying out diced electrophoresis gel (DEG) assay, which is a combination analysis of 2D-gel fluorometric assay and peptide mass fingerprinting,[29] using HMRef-αMan and lysate from an IDC specimen. We observed a single fluorescent spot on the gel, and this was identified as human cytosolic α-mannosidase 2C1 (MAN2C1) by peptide mass fingerprinting analysis (Figures 3f, S10 and Table S2). According to the Carbohydrate Active EnZYmes (CAZY) database, MAN2C1 belongs to glycoside hydrolase family 38 (GH38), and GH38 family α-mannosidase is likely to be inhibited by swainsonine.[30] Indeed, fluorescence increases of HMRef-αMan in cultured cells and surgical specimens were significantly inhibited in the presence of swainsonine, supporting the conclusion based on a DEG assay

https://dx.doi.org/10.1021/acscentsci.0c01189
ACS Cent. Sci. 2020, 6, 2217−2227

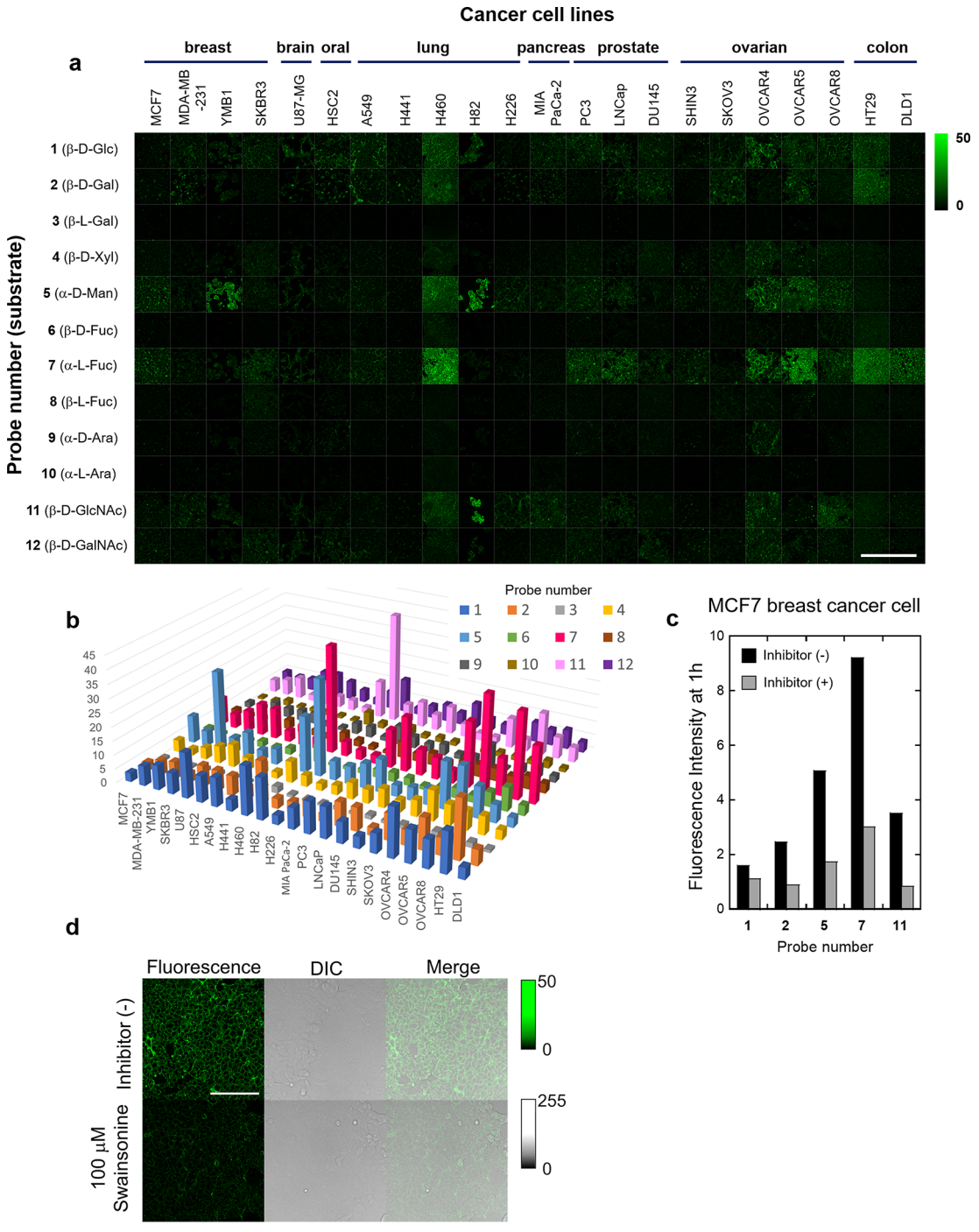

Figure 2. Comprehensive analysis of intact glycosidase activities in various living cancer cell lines. (a) Fluorescence imaging of glycosidase activities in 22 living cancer cell lines. All fluorescence images were captured 1 h after administration of each fluorescent probe. [fluorescent probe] = 10 μM. Scale bar, 400 μm. (b) Mapping of intracellular fluorescence intensities of each probe in 22 living cancer cell lines. (c) Fluorescence intensities of probes **1** (β-D-Glc), **2** (β-D-Gal), **5** (α-D-Man), **7** (α-L-Fuc), and **11** (β-D-GlcNAc) in MCF7 breast cancer cells in the presence and absence of each inhibitor. Black bars: fluorescence increase in the absence of inhibitor. Gray bars: fluorescence increase in the presence of inhibitor. All intensities were evaluated 1 h after administration of each probe and inhibitor. The inhibitors used were isofagomine for **1** (β-D-Glc), *N*-(*n*-nonyl) deoxygalactonoijirimycin for **2** (β-D-Gal), swainsonine for **5** (α-D-Man), deoxyfuconoijirimycin for **7** (α-L-Fuc), and PUGNAc for **11** (β-D-GlcNAc). [fluorescent probe] = 5 μM, [inhibitor] = 100 μM. (d) Fluorescence images of MCF7 cells incubated with probe **5** (α-D-Man) in the presence and absence of swainsonine. Scale bar, 100 μm.

that MAN2C1 is a promising biomarker for breast cancer imaging (Figure 3c and Figures S4−S5). For further confirmation, we evaluated the expression level of MAN2C1 in the specimens by immunohistochemical (IHC) staining. Normal mammary gland and fat tissues showed little MAN2C1 staining, whereas IDC and DCIS tissues showed strong staining (Figures 3g), indicating that MAN2C1 is overexpressed in breast cancer tissues. To our knowledge, overexpression of MAN2C1 in breast cancer has not previously been reported, and

https://dx.doi.org/10.1021/acscentsci.0c01189
ACS Cent. Sci. 2020, 6, 2217−2227

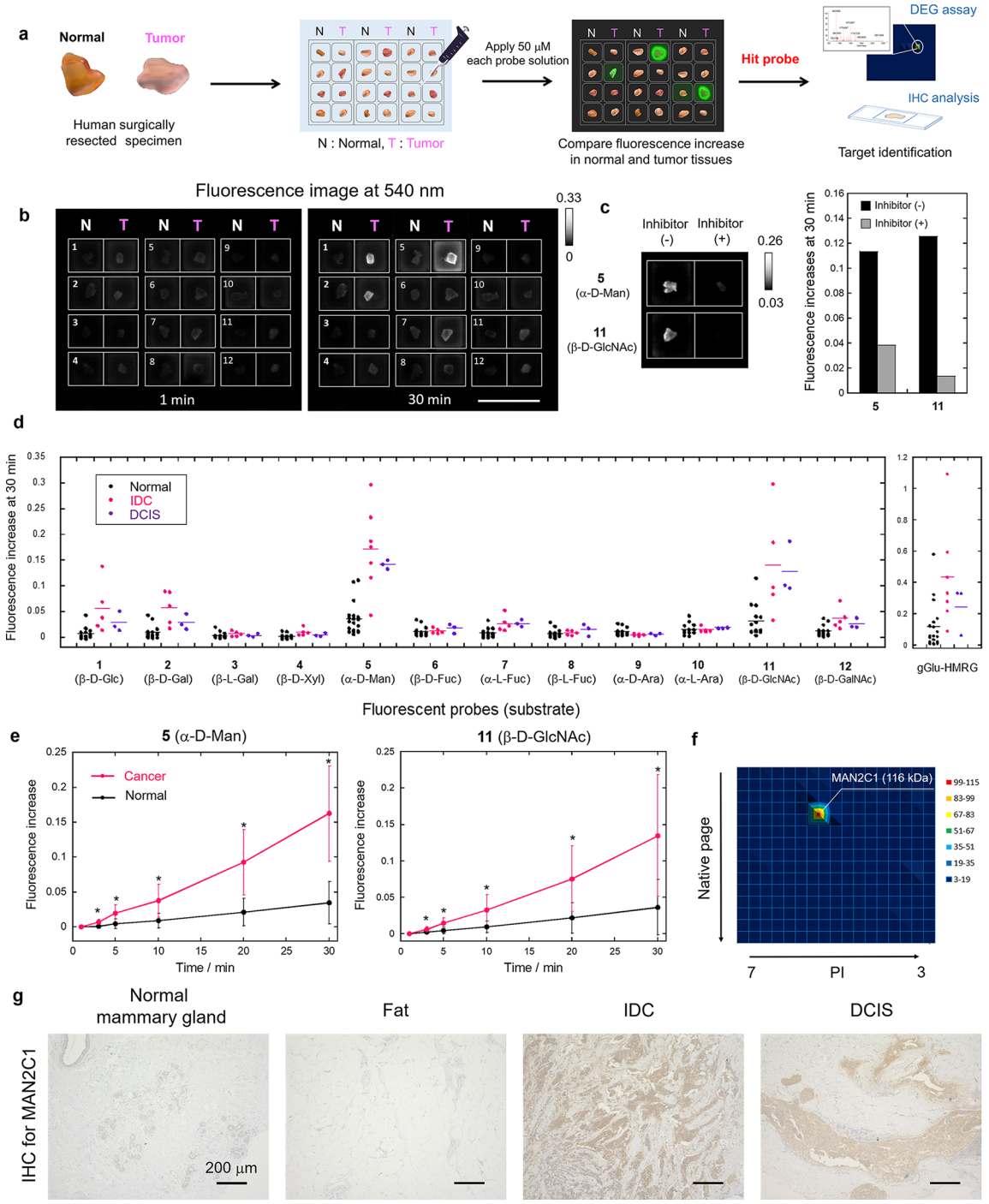

Figure 3. Screening of glycosidase-reactive fluorescent probes for the detection of breast tumors. (a) Flowchart of screening using human surgical normal tissue and tumor specimens. (b) Example of screening using surgically resected frozen human breast IDC and normal tissues. The compound number of the applied probe is shown on each well. Probe solution was prepared with PBS (−) containing 0.5% v/v DMSO as a cosolvent. [fluorescent probe] = 50 μM. Scale bar, 2 cm. (c) Fluorescence increase at 30 min in breast IDC tissues in the presence and absence of each inhibitor. Black bars: fluorescence increase in the absence of inhibitor. Gray bars: fluorescence increase in the presence of inhibitor. [fluorescent probe] = 50 μM, [swainsonine] = 500 μM for probe **5** (α-D-Man), [PUGNAc] = 500 μM for probe **11** (β-D-GlcNAc). (d) Comprehensive analysis of intact glycosidase activities in normal breast, IDC and DCIS tissues using 12 fluorescent probes or gGlu-HMRG (N = 14−20 for normal, N = 5−7 for IDC, N = 3 for DCIS). Fluorescence increase represent increase at 30 min from 1 min after addition of fluorescent probes. Black, pink, and purple dots represent fluorescence increases in normal breast, IDC and DCIS tissues, respectively. (e) Time-dependent fluorescence increase of probe **5** (α-D-Man) and **11** (β-D-GlcNAc) in breast normal and cancer tissues. Black lines represent fluorescence increases in normal breast tissues. Pink lines represent fluorescence increases in breast cancer (IDC + DCIS) tissues. Error bars represent s.d. *P < 0.05 by Welch's t-test. (f) DEG assay for IDC tissue using probe **5** (α-D-Man). MAN2C1 (116 kDa) was identified by peptide mass fingerprinting analysis from the fluorescent spot on 2D gel. (g) IHC staining for MAN2C1 in normal mammary gland, fat, IDC and DCIS tissues. Scale bars, 200 μm.

our findings represent the first evidence suggesting the potential utility of MAN2C1 as a biomarker of IDC and DCIS.

Application of the α-Mannosidase-Reactive Probe for Specific Demarcation of Breast Cancer. We next examined

https://dx.doi.org/10.1021/acscentsci.0c01189
ACS Cent. Sci. 2020, 6, 2217−2227

Table 1. Performance of Fluorescent Probes for the Detection of Breast Cancer[a]

Probes	Threshold value	PPV	NPV	Sensitivity	Specificity	AUC
HMRef-αMan	0.117	100%	95%	90%	100%	0.985
11 (β-D-GlcNAc)	0.083	78%	94%	89%	88%	0.896
gGlu-HMRG	0.216	67%	88%	80%	79%	0.832

[a]Threshold value, sensitivity and specificity of each probe were evaluated from the receiver operating characteristic curve (Figure S8). AUC, Area under the curve.

whether HMRef-αMan can visualize the boundaries of breast cancer lesions in relatively large surgically resected breast specimens. The specimens, which were expected to contain both breast IDC or DCIS and normal tissues, were incubated with a 50 μM PBS (−) solution of HMRef-αMan containing 0.5% v/v DMSO as a cosolvent, and fluorescence images were captured. Fluorescence activation was observed at specific regions of the specimens (Figure 4a and c). HE-staining indicated that the fluorescence-activated regions coincided well with pathologically diagnosed cancer cell-containing regions, while non-fluorescent regions were diagnosed as normal breast tissue (Figure 4). Notably, we successfully visualized tiny DCIS lesions (less than 1 mm in diameter) within 15 min, as exemplified by ROI (region of interest) #4, #6, #7, and #8 in the figures. Thus, HMRef-αMan can detect tiny cancerous lesions that are completely undetectable with the naked eye. We also evaluated the expression of MAN2C1 by means of IHC staining and confirmed that the pathologically diagnosed cancer regions exhibited higher MAN2C1 expression than normal regions (Figure 4b and f). These results indicate that MAN2C1 is overexpressed in IDC and DCIS tissues, and thus our α-mannosidase-reactive HMRef-αMan should be useful for the detection of breast cancer.

Evaluation of α-Mannosidase Activity in Benign Breast Lesions. Next, we evaluated the α-mannosidase activity in various benign breast lesions, including fibroadenoma (FA; the most frequently diagnosed breast benign lesion in young women[31,32]), phyllodes tumor (PT), and intracystic papilloma (ICP) (Figures S11 and S12). All these benign tumors exhibited strong fluorescence with HMRef-αMan, and the values of sensitivity and specificity for FA vs normal tissue were 100% (Figure S13). We also confirmed that HMRef-αMan is activated by MAN2C1 in FA tissues by means of DEG assay, as in the case of breast cancer (Figure S10 and Table S3) and established that MAN2C1 is significantly overexpressed in FA tissues by means of IHC analysis. MAN2C1 is also significantly overexpressed in other benign breast lesions, including intraductal papilloma (IDP) (Figure 5a). Thus, application of HMRef-αMan could identify FA regions (Figures 5b, c and S11), as well as PT and ICP in surgically resected breast specimens (Figure S12). These results indicate that HMRef-αMan is a universal biomarker for various malignant and benign lesions of the breast, and our probe can clearly distinguish these lesions from normal tissue regions.

Discrimination of Malignant and Benign Breast Lesions by Dual-Color Imaging. Since accurate discrimination of cancer and benign lesions is crucial to prevent misdiagnosis, we next examined whether HMRef-αMan can discriminate them. Interestingly, we found that HMRef-αMan tended to show greater fluorescence increases in FA tissues than IDC and DCIS tissues (Figures 6a, S14 and S15). Its sensitivity and specificity in binary classification (cancer/FA) were 90% and 80%, when the threshold value was set at 0.234 au (Figure S16). This result suggested that HMRef-αMan can be used to discriminate cancer and benign FA.

Considering that HMRef-αMan tends to show higher fluorescence increases in FA tissues than in IDC or DCIS malignant tissues ($P < 0.05$*), whereas gGlu-HMRG is similarly activated in both malignant and benign tissues ($P = 0.145$), we thought it might be possible to discriminate cancer and benign lesions by using a combination of α-mannosidase-reactive probe and GGT-reactive probe with different emission wavelengths (Figures 6a and S17). For this purpose, we newly synthesized a GGT-reactive fluorescent probe with emission in the red wavelength region, gGlu-2OMe SiR600, by conjugating a γ-glutamyl moiety to our recently reported scaffold fluorophore for activatable fluorescence probes for aminopeptidases, 2OMe SiR600.[33] This probe is well quenched via the photoinduced electron transfer (PeT) mechanism, but is converted to a highly fluorescent molecule upon reaction with GGT (Figure 6b). The utility of this new probe for the detection of GGT activity was evaluated and confirmed (Figure S18). Then, we used the combination of HMRef-αMan (green) and gGlu-2OMe SiR600 (red) to visualize the activities of α-mannosidase and GGT in normal, cancerous (IDC and DCIS), and benign (FA) breast tissues. As expected, FA tissue showed higher fluorescence activation than cancerous tissues in the green channel, while both cancer and FA tissues showed similar fluorescence activation in the red channel. On the other hand, normal breast tissues exhibited almost no activation in either channel. Therefore, in the composite image, normal regions were not fluorescent, cancer tissues were visualized in red, and FA tissues were visualized in yellow, thereby allowing the efficient optical discrimination of normal tissue, breast cancer, and benign lesions based on specific enzyme activities (Figures 6c, S19, and S20).

DISCUSSION

Fluorescence-guided detection of cancer is a promising approach to perform intraoperative assessment of surgical margins in BCS, and various types of fluorescent probes have been developed for detecting breast cancer by targeting upregulated enzymes or biomolecules.[12−17,34−37] We and other groups have focused on cancer-associated proteases as imaging targets for fluorescent probes to achieve rapid and high-contrast tumor visualization due to the high amplification of fluorescence by enzymatic turnover at lesion sites.[9,13,37−39]

In the present study, we turned to glycosidase activities, and synthesized 12 fluorescent probes for different glycosidases with the aim of finding a suitable biomarker enzyme in breast tumors. By means of our straightforward fluorescence imaging evaluation, we found that α-mannosidase activity is significantly enhanced in breast cancer and benign lesions, and our results indicate that the α-mannosidase-reactive probe, HMRef-αMan, is a promising fluorescent probe for rapid visualization of breast tumors. Compared to our previously reported probe gGlu-HMRG, HMRef-αMan shows higher sensitivity and specificity.

https://dx.doi.org/10.1021/acscentsci.0c01189
ACS Cent. Sci. 2020, 6, 2217−2227

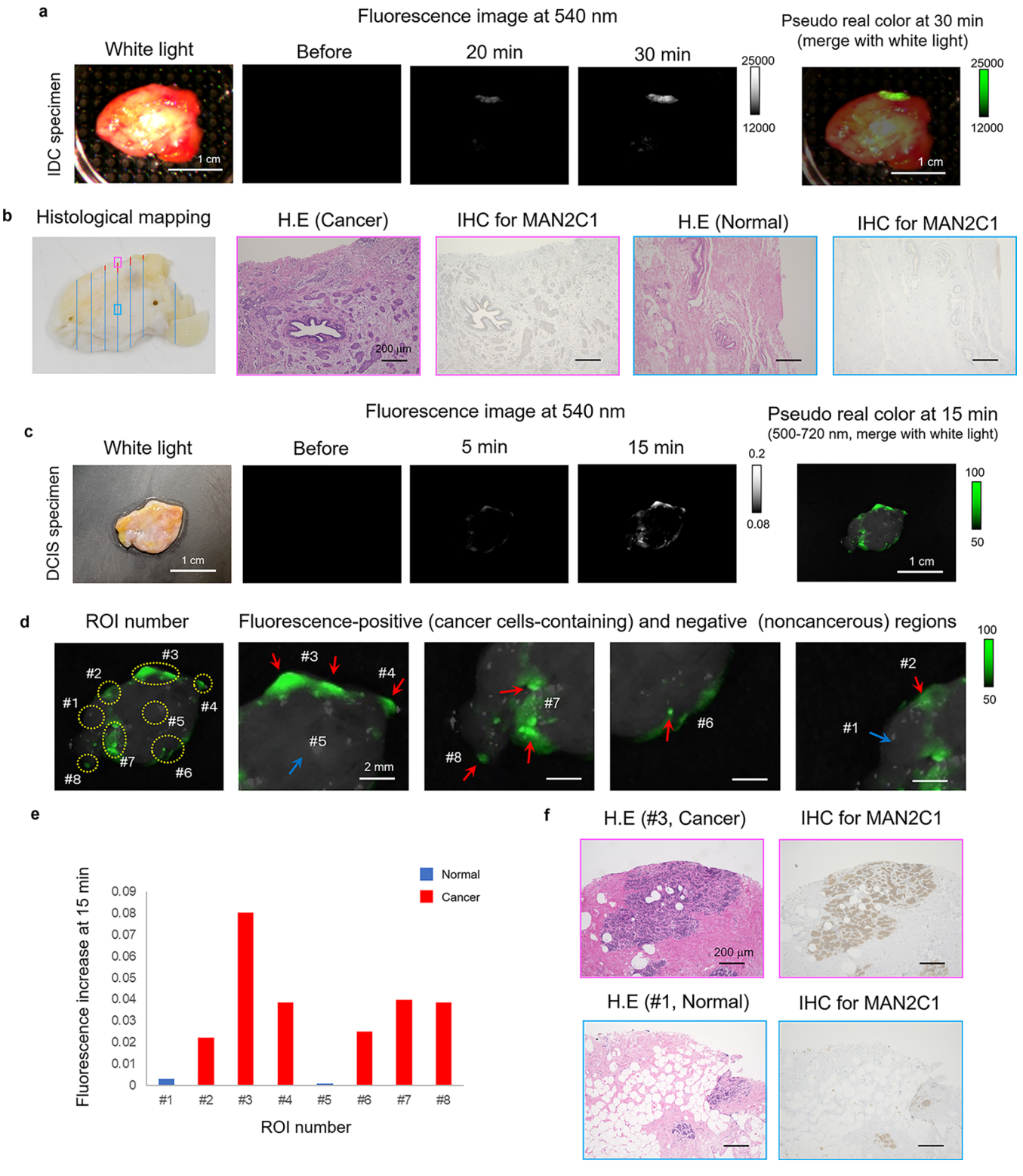

Figure 4. Application of α-mannosidase-reactive fluorescent probe to breast cancer-specific imaging. (a) Time-dependent fluorescence image of surgically resected fresh human IDC specimens containing both normal and cancer tissues after administration of HMRef-αMan. Probe solution was prepared with PBS (−) containing 0.5% v/v DMSO as a cosolvent. Scale bar, 1 cm. [fluorescent probe] = 50 μM. (b) Histological mapping of the specimen: red lines show IDC and blue lines show no tumor (left). Histological analysis and IHC analysis for MAN2C1 of boxed regions with strong fluorescence activation (pink box) or with no fluorescence activation (blue box). Scale bar, 200 μm. (c) Time-dependent fluorescence image of surgically resected frozen human DCIS specimen containing both normal and cancer tissues after administration of HMRef-αMan. Probe solution was prepared with PBS (−) containing 0.5% v/v DMSO as a cosolvent. Scale bar, 1 cm. [HMRef-αMan] = 50 μM. (d) ROI number of the evaluated DCIS specimen (left). Fluorescence-positive (red arrows) and -negative (blue arrow) regions (right). Cancer cells were detected in all fluorescence-positive ROIs by histological analysis. Scale bar, 2 mm. (e) Fluorescence increase at 15 min in each ROI. Red bars show cancer-cell-containing regions and blue bars show noncancerous regions. (f) Histological analysis and IHC analysis for MAN2C1 of ROI #3 with strong fluorescence activation (pink box) or ROI #1 with almost no fluorescence activation (blue box). Scale bar, 200 μm.

https://dx.doi.org/10.1021/acscentsci.0c01189
ACS Cent. Sci. 2020, 6, 2217−2227

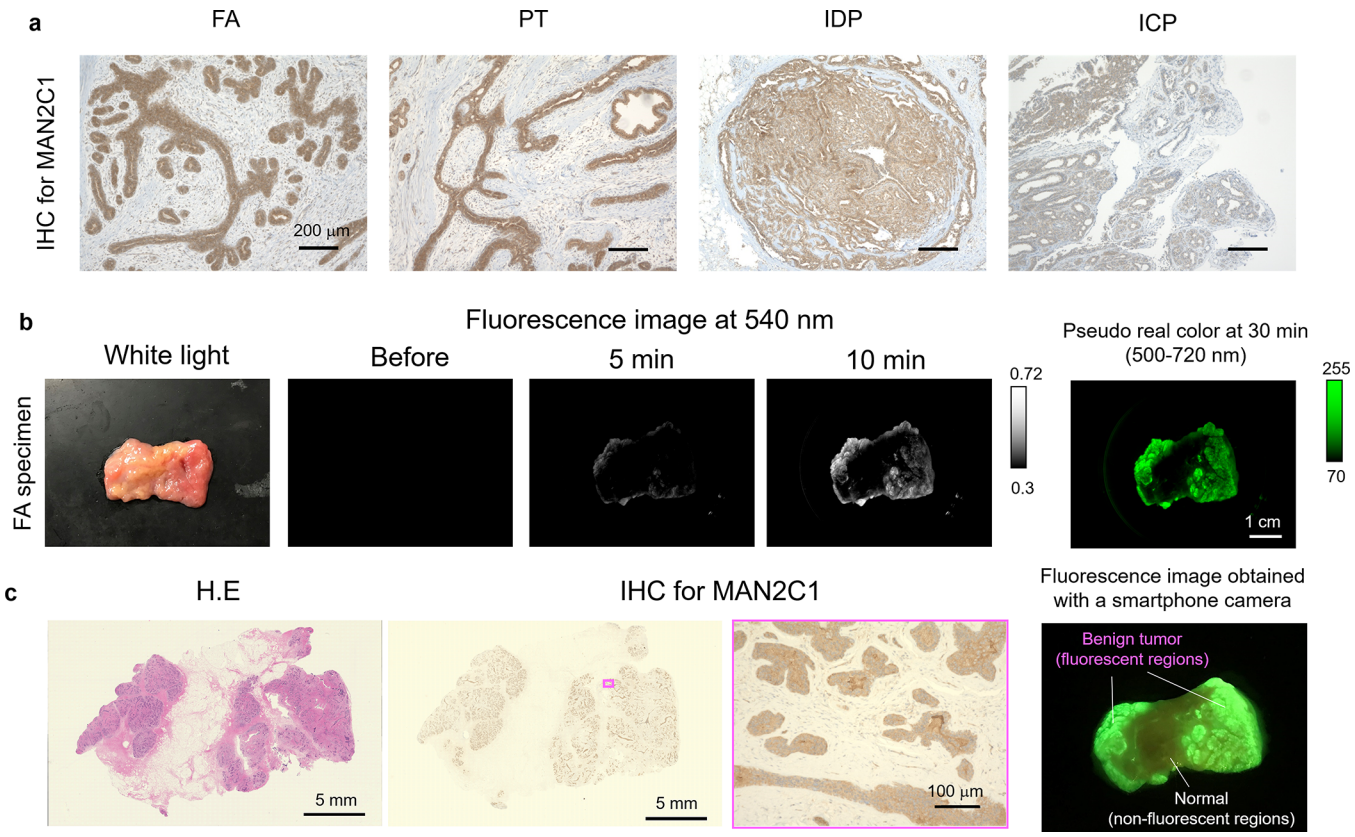

Figure 5. Application of α-mannosidase-reactive fluorescent probe for benign lesion-specific imaging of breast tissue. (a) IHC analysis for MAN2C1 in benign FA, PT, IDP, and ICP tissues of breast. Scale bars, 200 μm. (b) Time-dependent fluorescence image of surgically resected frozen human FA specimens containing both normal and FA tissues after administration of HMRef-αMan. Probe solution was prepared with PBS (−) containing 0.5% v/v DMSO as a cosolvent. Scale bar, 1 cm. [HMRef-αMan] = 50 μM. (c) Comparison of fluorescence localization with pathological HE-staining of the same specimen. Areas of increased fluorescence coincided well with pathologically confirmed FA regions (left). IHC staining for MAN2C1. Areas of increased fluorescence coincided well with the MAN2C1-positive regions (right). Fluorescence image was obtained 30 min after administration of probe by using a smartphone camera with 550 nm long pass filter.

In addition, it can visualize cancer tissues rapidly and with much higher tumor/nontumor ratios than can be achieved by always-on type probes, due to its highly amplified fluorescence resulting from turnover of α-mannosidase (Figure S21).[35,40−42] Indeed, we found that HMRef-αMan can rapidly detect tiny breast cancer lesions less than 1 mm in diameter. Since HMRef-αMan can be topically applied to the entire surface of surgical margins in a simple procedure that can be done without the aid of an experienced pathologist, this probe is expected to be a very powerful tool that can complement IFSA in BCS. Furthermore, we found that there are cancer specimens with weak GGT activity but high α-mannosidase activity in some cases, and vice versa. This result suggested that the combined use of both HMRef-αMan and gGlu-HMRG can achieve a more accurate discrimination between cancer and normal breast tissues.

Although the function of MAN2C1 in breast tumors has not been investigated in detail, MAN2C1 is involved in processing free oligosaccharides in the cytosol,[43] and its overexpression leads to modifications of the cytosolic pool of free oligomannosides.[44] MAN2C1 is also associated with cancer progression. MAN2C1 itself suppresses apoptosis in cancer cells regardless of its enzymatic activity;[45] it also attenuates PTEN function and activates PI3K/AKT signaling in PTEN-positive prostate cancer cells, thereby promoting prostate carcinogenesis (Figure S22).[46] We observed coexpression of MAN2C1, PTEN, and AKT-P (Ser473 phosphorylated AKT) in DCIS tissues, as in the case of PTEN-positive prostate cancer, suggesting that MAN2C1 may also attenuate PTEN function and increase AKT activation in breast cancer (Figure S23). This may imply that MAN2C1 overexpression in breast tumors could also be a potential therapeutic target.

It is noteworthy that this work is the first example of the discrimination of cancerous and benign breast lesions by optical imaging based on specific enzyme activities. As shown in Figure 6, we successfully discriminated the two types of tissues by dual-color, dual-target imaging with HMRef-αMan (green) and gGlu-2OMe SiR600 (red) probes. IHC analysis of the evaluated specimens in Figure 6c confirmed higher levels of MAN2C1 in benign FA tissues than in cancerous tissues, suggesting that the higher signal in benign tumors in this experiment is due to higher expression of MAN2C1 (Figure S24). A similar strategy might be applicable for discriminating various breast tumor pairs such as IDP and DCIS, or FA and PT, for which preoperative diagnosis is difficult.[47−50] We believe the concept of combining two or more probes targeting different specific enzyme activities is extremely promising for discriminating not only cancerous and benign tissues but also various tumor types in clinical settings.

CONCLUSION

In this study, we focus on glycosidase activities, with the aim of finding a new biomarker enzyme suitable for rapid, sensitive, and accurate detection of breast tumors during operation. We

https://dx.doi.org/10.1021/acscentsci.0c01189
ACS Cent. Sci. 2020, 6, 2217−2227

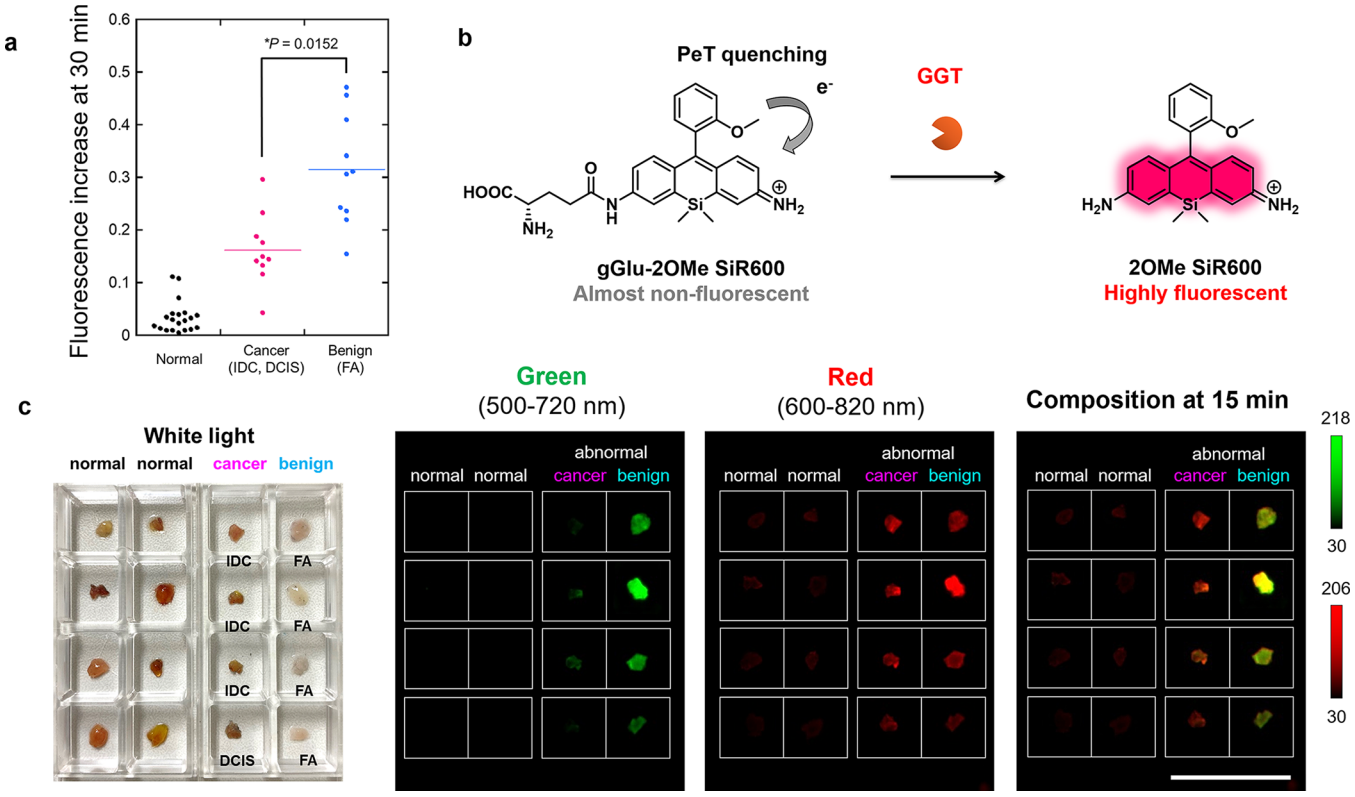

Figure 6. Application of fluorescent probes for the optical discrimination of breast cancer and benign breast lesions. (a) Fluorescence increase of HMRef-αMan in normal, cancer (IDC and DCIS) and benign (FA) breast tissues. The plots of normal, IDC, and DCIS show the same values as those in Figure 3d. HMRef-αMan tended to show higher fluorescence increases in benign FA tissues than in cancer tissues. *$P < 0.05$ by Welch's t-test (N = 20 for normal, N = 7 for IDC, N = 3 for DCIS, N = 10 for FA). [HMRef-αMan] = 50 μM. (b) A newly developed activatable red fluorescence probe for GGT, gGlu-2OMe SiR600. The initial fluorescence of the probe is well quenched via a PeT process. (c) White light image (left), and dual-color fluorescence images (right) of breast normal, cancer (IDC or DCIS) and benign (FA) tissues obtained with the combination of HMRef-αMan and gGlu-2OMe SiR600. Fluorescence images were captured 15 min after administration of both probes. Probe solution was prepared with PBS (−) containing 1% v/v DMSO as a cosolvent. Ex/Em = 465 nm/515 nm long pass for green, Ex/Em = 570 nm/610 nm long pass for red, [HMRef-αMan] = 50 μM, [gGlu-2OMe SiR600] = 50 μM. Scale bars, 2 cm.

synthesized a series of 12 fluorescent probes for sensitive detection of different glycosidase activities in living cells, and applied these probes to surgically resected breast specimens in order to find which would be the most effective. By means of our straightforward fluorescence imaging approach, we directly found that an α-mannosidase-reactive HMRef-αMan could rapidly detect breast cancer (less than 1 mm in diameter) with 90% sensitivity and 100% specificity. We identified the target of this probe as MAN2C1, a new biomarker enzyme, and confirmed that it is overexpressed in various breast tumors. We also found that fibroadenoma, which is the most common benign breast tumor in young woman, tends to have higher MAN2C1 activities than malignant breast cancer, whereas their GGT activities are similar. Based on this finding, we were able to achieve optical discrimination of malignant and benign tumors by combined application of two different-colored probes targeting MAN2C1 and GGT. These results clearly indicated that MAN2C1 is a new efficeint biomarker enzyme for rapid and accurate visualization of breast tumors.

METHODS

Reagents. All organic solvents and reagents were commercial products of guaranteed grade and were used without further purification. Water was doubly distilled and deionized by a Milli-Q water system before use.

Synthesis and Characterization of Compounds. Synthetic protocols of fluorescence probes are given in the Supporting Information. NMR spectra were recorded on a Bruker AVANCE III and 400 Nanobay at 400 MHz for ^{1}H NMR and 101 MHz for ^{13}C NMR. High-resolution mass spectra (HRMS) were measured with a MicroTOF (Bruker).

Cell Lines and Culture Conditions. Twenty-two established human cancer cell lines were used in this study. MCF7, MDA-MB-231, YMB1, SKBR3, H460, H441, H226, H82, LNCaP, PC3, DLD1, DU145, HT29, OVCAR4, OVCAR5, OVCAR8, SHIN3, and SKOV3 were cultured in RPMI-1640 (with L-glutamine and phenol red) and maintained at 37 °C in a humidified incubator under 5% CO_2 in air. A549, HSC2, and U87-MG were cultured in DMEM (high glucose with L-glutamine and phenol red) and maintained under the same conditions. All media were supplemented with 10% fetal bovine serum and 1% penicillin/streptomycin. MCF7, LNCaP, PC3, DU145, and A549 were obtained from RIKEN Cell Bank. MDA-MB-231, SKBR3, H460, H441, H226, H82, DLD1, HT29, SKOV3, and U87-MG were obtained from American Type Culture Collection. YMB1, MIA PaCa-2, and HSC2 were obtained from Japanese Collection of Research Bioresources Cell Bank. OVCAR4, OVCAR5, OVCAR8, and SHIN3 were provided by Prof. H. Kobayashi, NIH, U.S.A.

Confocal Imaging of Glycosidase Activity in Cultured Cancer Cells. For fluorescence microscopy, about 10 000 cells

https://dx.doi.org/10.1021/acscentsci.0c01189
ACS Cent. Sci. 2020, 6, 2217−2227

in 200 μL of medium supplemented with 10% fetal bovine serum and 1% penicillin/streptomycin were seeded in each well of an 8-well chamber (μ-Slide 8 well; Ibidi) and cultured for 1−2 days. The medium was replaced with 200 μL of phenol red- and serum-free RPMI-1640 or DMEM containing 10 μM glycosidase-reactive fluorescent probe. The plate was incubated at 37 °C for 1 h in a humidified incubator under 5% CO_2 in air, and differential interference contrast (DIC) and fluorescence images were obtained using a Leica Application Suite Advanced Fluorescence with a TCS SP5 X. The light source was a white light laser. Excitation and emission wavelengths were 498 nm/500−600 nm.

Clinical Samples. Sixty-five breast tumor patients underwent surgical treatment at the Ueo Breast Cancer Hospital. Twenty-four patients were enrolled for fluorescence imaging analysis for various tissues in breast (Figures 3−6, S6−S8, S11−S17, and S19−21, Tables 1 and S1), 2 patients were enrolled for DEG assay (Figures 3 and S10, Tables S2 and S3), and 65 patients were enrolled for immunohistochemical analysis (Figures 3−5, S11, S12, S23, and S24). Some patients were duplicated in plural analyses. Informed consent was obtained from all patients, and this study was approved by the local ethics committees. All experiments were performed in accordance with guidelines and regulations approved by ethics committees. All clinical and pathological data were obtained from medical records. Both fresh and frozen specimens were used in these experiments. Fresh surgical specimens were evaluated within 10 min after resection. Frozen specimens were frozen immediately after resection, stored at −80 °C, and thawed at room temperature before use.

Screening of Fluorescent Probes with Human Breast Surgical Specimens. A 50 μM solution of glycosidase-reactive fluorescent probe (200 μL) in PBS containing 0.5% v/v DMSO as a cosolvent was added to each well of an 8-well chamber (μ-Slide 8 well; Ibidi) containing a human surgical specimen (tumor or nontumor tissue). The fluorescence intensities and images of specimens were recorded with the Maestro *in vivo* imaging system (PerkinElmer) before and at 1, 3, 5, 10, 20, and 30 min after probe administration. The green filter setting (Ex/Em = 490 nm/550 nm long-pass) was used. The tunable filter was automatically increased in 10 nm increments from 500 to 720 nm, while the camera sequentially captured images at each wavelength interval. Fluorescence at 540 nm was extracted, and fluorescence intensities were quantified by drawing ROIs with the Maestro software. Exposure time was set at 100−50 ms depending on fluorescence intensity from specimens. The stage and lamp of the equipment were both set at position 1. Surgical specimens were frozen immediately after resection, stored at −80 °C, and thawed at room temperature before use in this experiment.

***Ex Vivo* Fluorescence Imaging of Human Breast Surgical Specimens Containing Both Tumor and Normal Tissues.** A 50 μM solution of HMRef-αMan (3−10 mL) in PBS containing 0.5% v/v DMSO as a cosolvent was added to a 3.5 or 5.0 cm dish containing a human surgical specimen so that the tissue was completely soaked with probe solution. Fluorescence images of fresh IDC specimens were recorded using an in-house-built portable fluorescence imager. The fluorescence images of frozen DCIS and FA specimens were recorded and evaluated as described above, using the Maestro *in vivo* imaging system. Exposure time was set at 100−20 ms depending on the level of fluorescence intensity from specimens. The stage and lamp of the equipment were both set at position 1 or 2. Fresh IDC specimens were evaluated 10 min after resection. DCIS and FA specimens were frozen immediately after resection, stored at −80 °C, and thawed at room temperature before use in this experiment.

Histological Analysis. Excised specimens were immediately fixed with 10% formaldehyde for at least 24 h. Formalin-fixed paraffin-embedded tissues were sectioned at 4 μm thickness and stained with hematoxylin and eosin for histopathological evaluation. Experienced pathologists examined each sample in a blind manner, and dysplasia and neoplasia were diagnosed according to the Japanese Breast Cancer Society criteria, 18th edition and WHO Classification of Tumor of the Breast, 5th edition. The distribution of carcinoma evaluated pathologically in the resected specimen was compared to that of fluorescence-positive regions.

Immunohistochemical Analysis of MAN2C1 Expression. Sections 4 μm thick were prepared as described above. Immunoperoxidase staining for MAN2C1 (mouse monoclonal antibody, Clone: C-4, Lot: B2216, Santa Cruz Biotechnology) was performed using a Ventana Benchmark XT (Ventana Medical Systems) automated slide-staining system. Sections were deparaffinized, pretreated with Cell Conditioning 1 (CC1, Ventana Medicals Systems), reacted with primary antibodies for 32 min at room temperature, visualized with a Ventana DAB detection kit (iView DAB detection kit), and counter-stained with Hematoxylin and Bluing Reagent. MAN2C1 antibody was diluted to 1/50 and used with an iVIEW DAB detection kit and Endogenous Biotin blocking kit (Ventana Medical Systems). As criteria to evaluate MAN2C1 expression, ≥10% positivity in cells was considered as positive.

Dual-Color Dual-Target Fluorescence Imaging of Surgically Resected Cancer and Benign Tissues. A 50 μM solution of HMRef-αMan and gGlu-2OMe SiR600 (200 μL) in PBS containing 1.0% v/v DMSO as a cosolvent was added to an 8-well chamber (μ-Slide 8 well; Ibidi) containing a human surgical cancer or benign specimen so that the tissue was completely soaked with probe solution. The fluorescence intensities and images of specimens were recorded and evaluated using the same method as above with the Maestro *in vivo* imaging system. Exposure time was set at 100−20 ms depending on the fluorescence intensity emitted by specimens. The stage and lamp of the equipment were both set at position 1. Surgical specimens were frozen immediately after resection, stored at −80 °C and thawed at room temperature before use in this experiment.

Statistical Analysis. Statistical analyses were performed with EZR software (Saitama Medical Centre, Jichi Medical University).[51] Sensitivity and specificity were evaluated from the receiver operating characteristic curves (see SI). Statistical comparisons between two samples were made using the unpaired Welch's *t*-test.

■ ASSOCIATED CONTENT

Supporting Information

The Supporting Information is available free of charge at https://pubs.acs.org/doi/10.1021/acscentsci.0c01189.

Fluorescence imaging using cultured cancer cells and human surgical specimens, evaluation of optical properties and response to α-mannosidase and GGT, list of detected proteins in DEG assay, ROC curves and sensitivity-specificity plots, IHC analysis, synthesis and characterization of compounds (PDF)

https://dx.doi.org/10.1021/acscentsci.0c01189
ACS Cent. Sci. 2020, 6, 2217−2227

AUTHOR INFORMATION

Corresponding Author

Yasuteru Urano − *Graduate School of Medicine and Graduate School of Pharmaceutical Sciences, The University of Tokyo, Bunkyo, Tokyo 113-0033, Japan; CREST, Japan Agency for Medical Research and Development, Chiyoda, Tokyo 100-0004, Japan*; Email: uranokun@m.u-tokyo.ac.jp

Authors

Kyohhei Fujita − *Graduate School of Medicine, The University of Tokyo, Bunkyo, Tokyo 113-0033, Japan;* orcid.org/0000-0002-1220-6327

Mako Kamiya − *Graduate School of Medicine, The University of Tokyo, Bunkyo, Tokyo 113-0033, Japan; PRESTO, Japan Science and Technology Agency, Kawaguchi, Saitama 332-0012, Japan;* orcid.org/0000-0002-5592-1849

Takafusa Yoshioka − *Graduate School of Medicine, The University of Tokyo, Bunkyo, Tokyo 113-0033, Japan*

Akira Ogasawara − *Graduate School of Pharmaceutical Sciences, The University of Tokyo, Bunkyo, Tokyo 113-0033, Japan*

Rumi Hino − *Daito Bunka University, Department of Sports and Health Science, Higashimatsuyama, Saitama 355-8501, Japan*

Ryosuke Kojima − *Graduate School of Medicine, The University of Tokyo, Bunkyo, Tokyo 113-0033, Japan; PRESTO, Japan Science and Technology Agency, Kawaguchi, Saitama 332-0012, Japan;* orcid.org/0000-0002-3792-9222

Hiroaki Ueo − *Ueo Breast Cancer Hospital, Oita, Oita 870-0887, Japan*

Complete contact information is available at: https://pubs.acs.org/10.1021/acscentsci.0c01189

Notes

The authors declare no competing financial interest.

ACKNOWLEDGMENTS

This research was supported in part by AMED under Grant Number JP19gm0710008 (to Y.U.), by JST/PRESTO Grant JPMJPR14F8 (to M.K.), by MEXT/JSPS KAKENHI Grants JP16H02606, JP26111012, and JP19H05632 (to Y.U.) and JP15H05951 "Resonance Bio", JP19H02826, and JP19K22242 (to M.K.), by JSPS Core-to-Core Program (Grant Number: JPJSCCA20170007), A. Advanced Research Networks, by Japan Foundation for Applied Enzymology (to M.K.), and The Naito Foundation (to M.K.), as well as a stipend from the Graduate Program for Leaders in Life Innovation (GPLLI) (to K.F.), World-leading INnovative Graduate Study program for Life Science and Technology (WINGS-LST) (to K.F.), Masason Foundation (to K.F.), and a JSPS stipend (to K.F.).

REFERENCES

(1) Bray, F.; Ferlay, J.; Soerjomataram, I.; Siegel, R. L.; Torre, L. A.; Jemal, A. Global cancer statistics 2018: GLOBOCAN estimates of incidence and mortality worldwide for 36 cancers in 185 countries. *Ca-Cancer J. Clin.* **2018**, *68* (6), 394−424.

(2) Fajdic, J.; Djurovic, D.; Gotovac, N.; Hrgovic, Z. Criteria and procedures for breast conserving surgery. *Acta Inform Med.* **2013**, *21* (1), 16−19.

(3) Kim, M. J.; Kim, C. S.; Park, Y. S.; Choi, E. H.; Han, K. D. The Efficacy of Intraoperative Frozen Section Analysis During Breast-Conserving Surgery for Patients with Ductal Carcinoma In Situ. *Breast Cancer: Basic Clin. Res.* **2016**, *10*, 205−210.

(4) Taxy, J. B. Frozen Section and the Surgical Pathologist: A Point of View. *Archives of Pathology & Laboratory Medicine* **2009**, *133* (7), 1135−1138.

(5) Fukamachi, K.; Ishida, T.; Usami, S.; Takeda, M.; Watanabe, M.; Sasano, H.; Ohuchi, N. Total-Circumference Intraoperative Frozen Section Analysis Reduces Margin-Positive Rate in Breast-Conservation Surgery. *Jpn. J. Clin. Oncol.* **2010**, *40* (6), 513−520.

(6) Frangioni, J. V. New Technologies for Human Cancer Imaging. *J. Clin. Oncol.* **2008**, *26* (24), 4012−4021.

(7) Löning, M.; Diddens, H.; Küpker, W.; Diedrich, K.; Hüttmann, G. Laparoscopic fluorescence detection of ovarian carcinoma metastases using 5-aminolevulinic acid-induced protoporphyrin IX. *Cancer* **2004**, *100* (8), 1650−1656.

(8) Alander, J. T.; Kaartinen, I.; Laakso, A.; Pätilä, T.; Spillmann, T.; Tuchin, V. V.; Venermo, M.; Välisuo, P. A review of indocyanine green fluorescent imaging in surgery. *Int. J. Biomed. Imaging* **2012**, *2012*, 940585−940585.

(9) Ueo, H.; Shinden, Y.; Tobo, T.; Gamachi, A.; Udo, M.; Komatsu, H.; Nambara, S.; Saito, T.; Ueda, M.; Hirata, H.; Sakimura, S.; Takano, Y.; Uchi, R.; Kurashige, J.; Akiyoshi, S.; Iguchi, T.; Eguchi, H.; Sugimachi, K.; Kubota, Y.; Kai, Y.; Shibuta, K.; Kijima, Y.; Yoshinaka, H.; Natsugoe, S.; Mori, M.; Maehara, Y.; Sakabe, M.; Kamiya, M.; Kakareka, J. W.; Pohida, T. J.; Choyke, P. L.; Kobayashi, H.; Ueo, H.; Urano, Y.; Mimori, K. Rapid intraoperative visualization of breast lesions with γ-glutamyl hydroxymethyl rhodamine green. *Sci. Rep.* **2015**, *5* (1), 12080.

(10) Onoyama, H.; Kamiya, M.; Kuriki, Y.; Komatsu, T.; Abe, H.; Tsuji, Y.; Yagi, K.; Yamagata, Y.; Aikou, S.; Nishida, M.; Mori, K.; Yamashita, H.; Fujishiro, M.; Nomura, S.; Shimizu, N.; Fukayama, M.; Koike, K.; Urano, Y.; Seto, Y. Rapid and sensitive detection of early esophageal squamous cell carcinoma with fluorescence probe targeting dipeptidylpeptidase IV. *Sci. Rep.* **2016**, *6* (1), 26399.

(11) Bremer, C.; Tung, C.-H.; Bogdanov, A.; Weissleder, R. Imaging of Differential Protease Expression in Breast Cancers for Detection of Aggressive Tumor Phenotypes. *Radiology* **2002**, *222* (3), 814−818.

(12) Verdoes, M.; Oresic Bender, K.; Segal, E.; van der Linden, W. A.; Syed, S.; Withana, N. P.; Sanman, L. E.; Bogyo, M. Improved Quenched Fluorescent Probe for Imaging of Cysteine Cathepsin Activity. *J. Am. Chem. Soc.* **2013**, *135* (39), 14726−14730.

(13) Miampamba, M.; Liu, J.; Harootunian, A.; Gale, A. J.; Baird, S.; Chen, S. L.; Nguyen, Q. T.; Tsien, R. Y.; González, J. E. Sensitive in vivo Visualization of Breast Cancer Using Ratiometric Protease-activatable Fluorescent Imaging Agent, AVB-620. *Theranostics* **2017**, *7* (13), 3369−3386.

(14) Poreba, M.; Rut, W.; Vizovisek, M.; Groborz, K.; Kasperkiewicz, P.; Finlay, D.; Vuori, K.; Turk, D.; Turk, B.; Salvesen, G. S.; Drag, M. Selective imaging of cathepsin L in breast cancer by fluorescent activity-based probes. *Chemical Science* **2018**, *9* (8), 2113−2129.

(15) Tholen, M.; Yim, J. J.; Groborz, K.; Yoo, E.; Martin, B. A.; van den Berg, N. S.; Drag, M.; Bogyo, M. Design of Optical-Imaging Probes by Screening of Diverse Substrate Libraries Directly in Disease-Tissue Extracts. *Angew. Chem., Int. Ed.* **2020**, *59*, 19143−19152.

(16) Whitley, M. J.; Cardona, D. M.; Lazarides, A. L.; Spasojevic, I.; Ferrer, J. M.; Cahill, J.; Lee, C.-L.; Snuderl, M.; Blazer, D. G.; Hwang, E. S.; Greenup, R. A.; Mosca, P. J.; Mito, J. K.; Cuneo, K. C.; Larrier, N. A.; O'Reilly, E. K.; Riedel, R. F.; Eward, W. C.; Strasfeld, D. B.; Fukumura, D.; Jain, R. K.; Lee, W. D.; Griffith, L. G.; Bawendi, M. G.; Kirsch, D. G.; Brigman, B. E. A mouse-human phase 1 co-clinical trial of a protease-activated fluorescent probe for imaging cancer. *Sci. Transl. Med.* **2016**, *8* (320), 320ra4−320ra4.

(17) Olson, E. S.; Jiang, T.; Aguilera, T. A.; Nguyen, Q. T.; Ellies, L. G.; Scadeng, M.; Tsien, R. Y. Activatable cell penetrating peptides linked to nanoparticles as dual probes for in vivo fluorescence and MR imaging of proteases. *Proc. Natl. Acad. Sci. U. S. A.* **2010**, *107* (9), 4311−4316.

(18) Urano, Y.; Sakabe, M.; Kosaka, N.; Ogawa, M.; Mitsunaga, M.; Asanuma, D.; Kamiya, M.; Young, M. R.; Nagano, T.; Choyke, P. L.; Kobayashi, H. Rapid Cancer Detection by Topically Spraying a γ-Glutamyltranspeptidase−Activated Fluorescent Probe. *Sci. Transl. Med.* **2011**, *3* (110), 110ra119−110ra119.

(19) Sakabe, M.; Asanuma, D.; Kamiya, M.; Iwatate, R. J.; Hanaoka, K.; Terai, T.; Nagano, T.; Urano, Y. Rational Design of Highly Sensitive

Fluorescence Probes for Protease and Glycosidase Based on Precisely Controlled Spirocyclization. *J. Am. Chem. Soc.* **2013**, *135* (1), 409−414.
(20) Shinden, Y.; Ueo, H.; Tobo, T.; Gamachi, A.; Utou, M.; Komatsu, H.; Nambara, S.; Saito, T.; Ueda, M.; Hirata, H.; Sakimura, S.; Takano, Y.; Uchi, R.; Kurashige, J.; Akiyoshi, S.; Iguchi, T.; Eguchi, H.; Sugimachi, K.; Kubota, Y.; Kai, Y.; Shibuta, K.; Kijima, Y.; Yoshinaka, H.; Natsugoe, S.; Mori, M.; Maehara, Y.; Sakabe, M.; Kamiya, M.; Kakareka, J. W.; Pohida, T. J.; Choyke, P. L.; Kobayashi, H.; Ueo, H.; Urano, Y.; Mimori, K. Rapid diagnosis of lymph node metastasis in breast cancer using a new fluorescent method with γ-glutamyl hydroxymethyl rhodamine green. *Sci. Rep.* **2016**, *6* (1), 27525.
(21) Vajaria, B. N.; Patel, P. S. Glycosylation: a hallmark of cancer? *Glycoconjugate J.* **2017**, *34* (2), 147−156.
(22) Cheng, T. C.; Tu, S. H.; Chen, L. C.; Chen, M. Y.; Chen, W. Y.; Lin, Y. K.; Ho, C. T.; Lin, S. Y.; Wu, C. H.; Ho, Y. S. Down-regulation of α-L-fucosidase 1 expression confers inferior survival for triple-negative breast cancer patients by modulating the glycosylation status of the tumor cell surface. *Oncotarget* **2015**, *6* (25), 21283−300.
(23) Ezawa, I.; Sawai, Y.; Kawase, T.; Okabe, A.; Tsutsumi, S.; Ichikawa, H.; Kobayashi, Y.; Tashiro, F.; Namiki, H.; Kondo, T.; Semba, K.; Aburatani, H.; Taya, Y.; Nakagama, H.; Ohki, R. Novel p53 target gene FUCA1 encodes a fucosidase and regulates growth and survival of cancer cells. *Cancer Sci.* **2016**, *107* (6), 734−45.
(24) Gil-Martín, E.; Gil-Seijo, S.; Nieto-Novoa, C.; Fernández-Briera, A. Elevation of acid glycosidase activities in thyroid and gastric tumors. *Int. J. Biochem. Cell Biol.* **1996**, *28* (6), 651−657.
(25) Bosmann, H. B.; Hall, T. C. Enzyme activity in invasive tumors of human breast and colon. *Proc. Natl. Acad. Sci. U. S. A.* **1974**, *71* (5), 1833−1837.
(26) Asanuma, D.; Sakabe, M.; Kamiya, M.; Yamamoto, K.; Hiratake, J.; Ogawa, M.; Kosaka, N.; Choyke, P. L.; Nagano, T.; Kobayashi, H.; Urano, Y. Sensitive β-galactosidase-targeting fluorescence probe for visualizing small peritoneal metastatic tumours in vivo. *Nat. Commun.* **2015**, *6* (1), 6463.
(27) Matsuzaki, H.; Kamiya, M.; Iwatate, R. J.; Asanuma, D.; Watanabe, T.; Urano, Y. Novel Hexosaminidase-Targeting Fluorescence Probe for Visualizing Human Colorectal Cancer. *Bioconjugate Chem.* **2016**, *27* (4), 973−981.
(28) Rivas, C.; Kamiya, M.; Urano, Y. A novel sialidase-activatable fluorescence probe with improved stability for the sensitive detection of sialidase. *Bioorg. Med. Chem. Lett.* **2020**, *30* (2), 126860.
(29) Komatsu, T.; Hanaoka, K.; Adibekian, A.; Yoshioka, K.; Terai, T.; Ueno, T.; Kawaguchi, M.; Cravatt, B. F.; Nagano, T. Diced Electrophoresis Gel Assay for Screening Enzymes with Specified Activities. *J. Am. Chem. Soc.* **2013**, *135* (16), 6002−6005.
(30) Costanzi, E.; et al. Cloning and expression of mouse cytosolic α-mannosidase (Man2c1). *Biochim. Biophys. Acta, Gen. Subj.* **2006**, *1760*, 1580−1586.
(31) Costanzi, E.; Balducci, C.; Cacan, R.; Duvet, S.; Orlacchio, A.; Beccari, T. Cloning and expression of mouse cytosolic alpha-mannosidase (Man2c1). *Biochim. Biophys. Acta, Gen. Subj.* **2006**, *1760* (10), 1580−6.
(32) Sosin, M.; Pulcrano, M.; Feldman, E. D.; Patel, K. M.; Nahabedian, M. Y.; Weissler, J. M.; Rodriguez, E. D. Giant juvenile fibroadenoma: a systematic review with diagnostic and treatment recommendations. *Gland Surg* **2015**, *4* (4), 312−321.
(33) Ogasawara, A.; Kamiya, M.; Sakamoto, K.; Kuriki, Y.; Fujita, K.; Komatsu, T.; Ueno, T.; Hanaoka, K.; Onoyama, H.; Abe, H.; Tsuji, Y.; Fujishiro, M.; Koike, K.; Fukayama, M.; Seto, Y.; Urano, Y. Red Fluorescence Probe Targeted to Dipeptidylpeptidase-IV for Highly Sensitive Detection of Esophageal Cancer. *Bioconjugate Chem.* **2019**, *30* (4), 1055−1060.
(34) Withana, N. P.; Garland, M.; Verdoes, M.; Ofori, L. O.; Segal, E.; Bogyo, M. Labeling of active proteases in fresh-frozen tissues by topical application of quenched activity-based probes. *Nat. Protoc.* **2016**, *11* (1), 184−91.
(35) Tanei, T.; Pradipta, A. R.; Morimoto, K.; Fujii, M.; Arata, M.; Ito, A.; Yoshida, M.; Saigitbatalova, E.; Kurbangalieva, A.; Ikeda, J.-I.; Morii, E.; Noguchi, S.; Tanaka, K. Cascade Reaction in Human Live Tissue Allows Clinically Applicable Diagnosis of Breast Cancer Morphology. *Adv. Sci. (Weinh)* **2019**, *6* (2), 1801479−1801479.
(36) Tummers, Q. R. J. G.; Hoogstins, C. E. S.; Gaarenstroom, K. N.; de Kroon, C. D.; van Poelgeest, M. I. E.; Vuyk, J.; Bosse, T.; Smit, V. T. H. B. M.; van de Velde, C. J. H.; Cohen, A. F.; Low, P. S.; Burggraaf, J.; Vahrmeijer, A. L. Intraoperative imaging of folate receptor alpha positive ovarian and breast cancer using the tumor specific agent EC17. *Oncotarget* **2016**, *7* (22), 32144−32155.
(37) Mahmood, U.; Weissleder, R. Near-Infrared Optical Imaging of Proteases in Cancer. *Molecular Cancer Therapeutics* **2003**, *2* (5), 489−496.
(38) Kawatani, M.; Yamamoto, K.; Yamada, D.; Kamiya, M.; Miyakawa, J.; Miyama, Y.; Kojima, R.; Morikawa, T.; Kume, H.; Urano, Y. Fluorescence Detection of Prostate Cancer by an Activatable Fluorescence Probe for PSMA Carboxypeptidase Activity. *J. Am. Chem. Soc.* **2019**, *141* (26), 10409−10416.
(39) Jiang, T.; Olson, E. S.; Nguyen, Q. T.; Roy, M.; Jennings, P. A.; Tsien, R. Y. Tumor imaging by means of proteolytic activation of cell-penetrating peptides. *Proc. Natl. Acad. Sci. U. S. A.* **2004**, *101* (51), 17867−17872.
(40) Poellinger, A.; Burock, S.; Grosenick, D.; Hagen, A.; Lüdemann, L.; Diekmann, F.; Engelken, F.; Macdonald, R.; Rinneberg, H.; Schlag, P.-M. Breast Cancer: Early- and Late-Fluorescence Near-Infrared Imaging with Indocyanine Green—A Preliminary Study. *Radiology* **2011**, *258* (2), 409−416.
(41) Zhang, C.; Mao, Y.; Wang, K.; Tian, J. The identification of breast cancer by Near-Infrared fluorescence imaging with methylene blue. *J. Clin. Oncol.* **2018**, *36* (15_suppl), e12591−e12591.
(42) Judy, R. P.; Keating, J. J.; DeJesus, E. M.; Jiang, J. X.; Okusanya, O. T.; Nie, S.; Holt, D. E.; Arlauckas, S. P.; Low, P. S.; Delikatny, E. J.; Singhal, S. Quantification of tumor fluorescence during intraoperative optical cancer imaging. *Sci. Rep.* **2015**, *5* (1), 16208.
(43) Suzuki, T.; Hara, I.; Nakano, M.; Shigeta, M.; Nakagawa, T.; Kondo, A.; Funakoshi, Y.; Taniguchi, N. Man2C1, an alpha-mannosidase, is involved in the trimming of free oligosaccharides in the cytosol. *Biochem. J.* **2006**, *400* (1), 33−41.
(44) Bernon, C.; Carré, Y.; Kuokkanen, E.; Slomianny, M.-C.; Mir, A.-M.; Krzewinski, F.; Cacan, R.; Heikinheimo, P.; Morelle, W.; Michalski, J.-C.; Foulquier, F.; Duvet, S. Overexpression of Man2C1 leads to protein underglycosylation and upregulation of endoplasmic reticulum-associated degradation pathway. *Glycobiology* **2011**, *21* (3), 363−375.
(45) Wang, L.; Suzuki, T. Dual Functions for Cytosolic α-Mannosidase (Man2C1): ITS DOWN-REGULATION CAUSES MITOCHONDRIA-DEPENDENT APOPTOSIS INDEPENDENTLY OF ITS α-MANNOSIDASE ACTIVITY. *J. Biol. Chem.* **2013**, *288* (17), 11887−11896.
(46) He, L.; Fan, C.; Kapoor, A.; Ingram, A. J.; Rybak, A. P.; Austin, R. C.; Dickhout, J.; Cutz, J.-C.; Scholey, J.; Tang, D. α-Mannosidase 2C1 attenuates PTEN function in prostate cancer cells. *Nat. Commun.* **2011**, *2* (1), 307.
(47) Stoffel, E.; Becker, A. S.; Wurnig, M. C.; Marcon, M.; Ghafoor, S.; Berger, N.; Boss, A. Distinction between phyllodes tumor and fibroadenoma in breast ultrasound using deep learning image analysis. *Eur. J. Radiol Open* **2018**, *5*, 165−170.
(48) Yilmaz, E.; Sal, S.; Lebe, B. Differentiation of phyllodes tumors versus fibroadenomas. *Acta Radiol.* **2002**, *43* (1), 34−39.
(49) Guray, M.; Sahin, A. A. Benign breast diseases: classification, diagnosis, and management. *Oncologist* **2006**, *11* (5), 435−49.
(50) Rozentsvayg, E.; Carver, K.; Borkar, S.; Mathew, M.; Enis, S.; Friedman, P. Surgical excision of benign papillomas diagnosed with core biopsy: a community hospital approach. *Radiol Res. Pract* **2011**, *2011*, 679864.
(51) Kanda, Y. Investigation of the freely available easy-to-use software 'EZR' for medical statistics. *Bone Marrow Transplant.* **2013**, *48* (3), 452−458.

https://dx.doi.org/10.1021/acscentsci.0c01189
ACS Cent. Sci. 2020, 6, 2217−2227